A new framework for using weather-sensitive surplus power reserves in critical infrastructure

Fallon, J. ORCID: https://orcid.org/0000-0002-6321-7456, Brayshaw, D. ORCID: https://orcid.org/0000-0002-3927-4362, Methven, J. ORCID: https://orcid.org/0000-0002-7636-6872, Jensen, K. and Krug, L. (2023) A new framework for using weather-sensitive surplus power reserves in critical infrastructure. Meteorological Applications, 30 (6). e2158. ISSN 1469-8080 doi: https://doi.org/10.1002/met.2158 Available at https://centaur.reading.ac.uk/114191/

Received: 2 December 2022 | Revised: 20 June 2023 | Accepted: 2 October 2023

DOI: 10.1002/met.2158

Meteorological Applications
Science and Technology for Weather and Climate
Open Access
RMetS

RESEARCH ARTICLE

A new framework for using weather-sensitive surplus power reserves in critical infrastructure

James Fallon[1] | David Brayshaw[1] | John Methven[1] | Kjeld Jensen[2] | Louise Krug[2]

[1]Department of Meteorology, University of Reading, Reading, UK

[2]Applied Research, British Telecommunications plc, London, UK

Correspondence
James Fallon, Department of Meteorology, University of Reading, Reading, Berkshire RG6 6BB, UK.
Email: j.fallon@pgr.reading.ac.uk

Funding information
Natural Environment Research Council, Grant/Award Number: F4114908

Abstract

Reserve power systems are widely used to provide power to critical infrastructure systems in the event of power outages. The reserve power system may be subject to regulation, typically focussing on a strict operational time commitment, but the energy involved in supplying reserve power may be highly variable. For example, if heating or cooling is involved, energy consumption may be strongly influenced by prevailing weather conditions and seasonality. Replacing legacy assets (often diesel generators) with modern technologies could offer potential benefits and services back to the wider electricity system when not in use, therefore supporting a transition to low-carbon energy networks. Drawing on the Great Britain telecommunications systems as an example, this paper demonstrates that meteorological reanalyses can be used to evaluate capacity requirements to maintain the regulated target of 5-days operational reserve. Across three case-study regions with diverse weather sensitivities, infrastructure with cooling-driven electricity demand is shown to increase energy consumption during summer, thus determining the overall capacity of the reserve required and the availability of 'surplus' capacity. Lower risk tolerance is shown to lead to a substantial cost increase in terms of capacity required but also enhanced opportunities for surplus capacity. The use of meteorological forecast information is shown to facilitate increased surplus capacity. Availability of surplus capacity is compared to a measure of supply–stress (demand-net-wind) on the wider energy network. For infrastructure with cooling-driven demand (typical of most UK telecommunication assets), it is shown that surplus availability peaks during periods of supply–stress, offering the greatest potential benefit to the national electricity grid.

KEYWORDS

climate risk, critical infrastructure, degree days, electricity demand, energy reanalysis, energy storage, forecast value, reserve power

1 | INTRODUCTION

Critical infrastructures are facilities necessary for a country to function or protect against danger to the public; for example, hospitals, transport services and communications infrastructure (CPNI, 2021). It is therefore vital that the operation of critical infrastructure is resilient to a wide spectrum of risks including external threats (such as threats from human conflict, extreme weather events and cyber attacks) and systemic threats (organizational or equipment failure, or long-term unsustainable practices (Guthrie & Konaris, 2012)).

Energy sector adaptation and mitigation of climate and ecological breakdown can complement aims to improve living standards, but requires a shift towards prioritization of energy sufficiency and global energy redistribution (Kikstra et al., 2021; Millward-Hopkins et al., 2020). In mid- and high-income nations, maintaining the operation of critical infrastructure in the event of electrical power loss is typically achieved through dedicated reserve generation capacity and offers strong social and economic benefits (Chawla et al., 2018; Guerrero et al., 2007). Ensuring the reliability of existing reserve systems and a global roll-out is therefore paramount to supporting a range of sustainable development goals.

On-site reserve is typically designed to provide a predefined level of resilience, for example, a specific operational time commitment for delivering a minimum N-days of power in the event of an outage. To date, most of this reserve has been provided via fossil fuel (gas or diesel) generators. However, to improve performance and achieve carbon emission reductions, new reserve generation systems based partially or fully on storage technologies, such as lithium-ion batteries or hydrogen fuel cells, can be considered to supplement and replace ageing reserve power fleets (Borzenko & Dunikov, 2017; Li, Niu, et al., 2018). Lifetime costs of these new technologies have already reduced substantially over recent decades and are projected to reduce significantly from 2020 to 2050 (Li, Lu, et al., 2018; Schmidt et al., 2019).

Flexible use of decarbonized reserve generation capacity may also offer wider benefits to national power systems. Currently, critical infrastructure reserve power supplies are typically rarely utilized and operate only in unusual situations when normal power supply is interrupted. However, as national-scale electricity networks seek to integrate ever larger shares of weather-dependent renewables (i.e., wind and solar power), the need for ancillary services (such as short-term operating reserve (National Grid ESO, 2019)) to manage weather risk increases. Flexible use of reserve generation capacity, when it is not required for its primary 'backup' role, could help to provide many of these valuable ancillary services.

Weather-driven models of energy demand are well established, with published literature typically focussing on national electricity grid demand (Taylor & Buizza, 2003). Studies on specific sectors can apply more complex models embedding different physical responses, for example in residential heating (Fumo & Rafe Biswas, 2015). Weber et al. (2018) demonstrate climate change impacts on backup energy storage considered at a continental scale in Europe. However, we address a perceived gap in published literature for the application of meteorological data to understanding drivers of critical infrastructure demand, making linkage to weather and climate risk to the reserve power infrastructure. Additionally, the exploration of 'surplus' capacity (introduced in Figure 1) is novel and opportune.

This paper, therefore, investigates the extent to which rarely-used critical infrastructure reserve power supplies can be released as ancillary services back to the wider power system, without compromising resilience. Specifically, we seek periods of 'surplus capacity' where the anticipated 5-day consumption of the protected critical infrastructure asset is less than the total installed backup generation capacity, although this concept can be applied to a more generalized N-day case.

The additional revenue derived by identifying and allocating surplus capacity in this way may support both the security and decarbonization of the wider grid, whilst offsetting some of the installation costs of the reserve power supply technology itself (Mustafa et al., 2021).

The paper is structured as follows: the underlying datasets are described in Section 2; weather-driven models of GB telecommunication systems' electricity consumption are developed using empirical data spanning 2016–2020 in Sections 3 and 4; in Section 5, these models are then applied to a longer 41-year temperature dataset to establish an extended baseline climatology of consumption over time. The resulting consumption climatology is then used to address the following scientific challenges:

1. To understand and quantify how the total reserve energy capacity required for the GB telecommunication system is impacted by differing levels of risk tolerance. (Sections 5.2 and 5.3).
2. To assess and understand how the total reserve energy capacity varies seasonally and hence to identify periods and quantities of surplus capacity available, given an expressed risk tolerance. (Sections 5.4–5.6).
3. To understand how the availability of surplus capacity relates to supply stress on the wider electricity network. (Section 5.7).

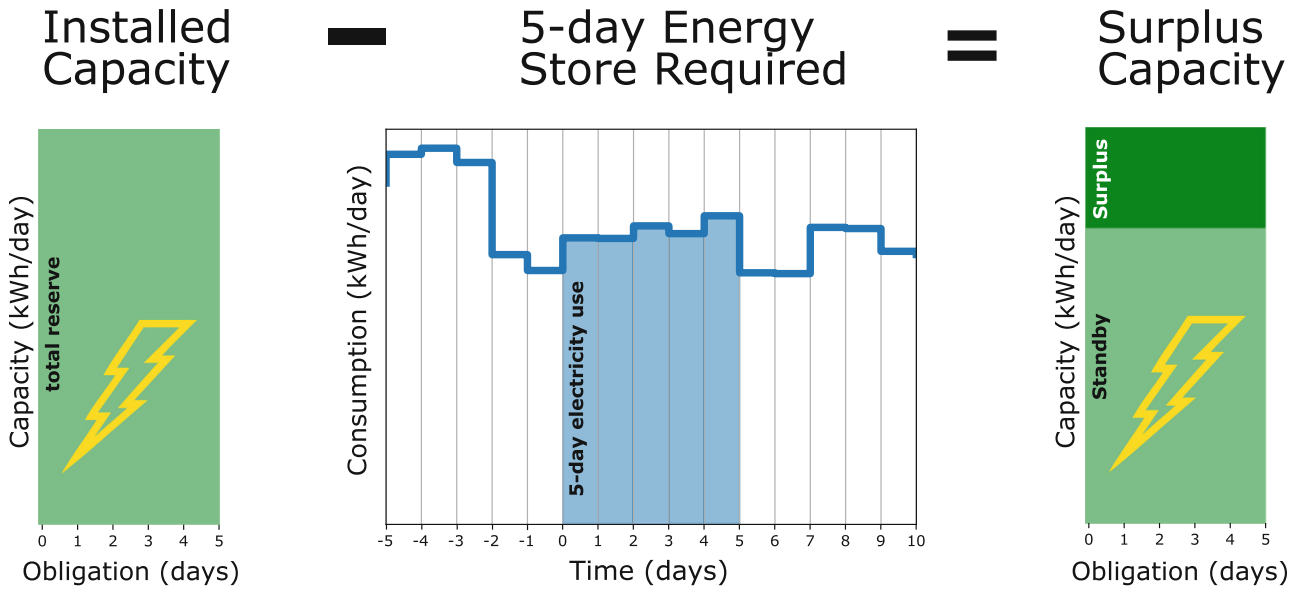

FIGURE 1 Schematic demonstrating the concept of surplus capacity, in the specific case of a 5-day reserve commitment. A critical infrastructure system has a fixed capacity of installed reserve (shown left shaded light green, height given in units of capacity per day and width in the delivery obligation time). Outside of the periods with very high infrastructure demand, the 5-day consumption (light blue) is some amount less than the installed capacity, leaving a portion of 'surplus' (dark green). If this surplus can be accurately anticipated, it may be utilized for other purposes without impacting the N-day reserve delivery commitment.

2 | DATASETS

We develop a temperature-driven model of telecommunications service provider BT's infrastructure electricity demand, based on data spanning 2016 to 2020. For context, BT uses just under 1% of UK electric grid energy, whilst overall healthcare electricity consumption in the UK is just under 0.5%.[1] The model's key features reflect those observed in the metered infrastructure demand datasets: weekday patterns driven by human behaviour and day-to-day variability largely explained by cooling power requirements. Analyses are conducted at both regional and national aggregate levels, with regions corresponding to the 14 British *Distribution Network Operator* geographic zones (National Grid ESO, 2020).

In this section we describe the datasets used, specifically: BT electricity consumption data (2.1), temperature records (2.2) and nation-wide electricity consumption and renewable generation (2.3).

2.1 | Infrastructure electricity demand

Metered infrastructure electricity demand data is shown in Figure 2a (quality control has removed unphysical readings). Data is anonymized to preserve sensitive information. The significant features are an overall downward trend related to operational energy efficiency improvements over time, substantial peaks in the summer (in particular, due to increased cooling requirements for network equipment locations) and smaller increases in the winter months due to heating requirements. There is also a weekday pattern in infrastructure demand, with weekends being slightly lower than the workdays (on average by 1%), as seen in Figure 2b. The impact of weekday variability on total infrastructure metered demand measured in each region is between 2.5% to 4.9%.

In the present context, we seek to understand and model the impact of meteorological drivers on BT's consumption. It is therefore desirable to remove the effects of long-term technological and behavioural trends and patterns such as the day-of-the-week effect. This process is described in Figure 2 and Equation 1:

$$\mathcal{D}(t) = \frac{D(t)}{D_{\text{weekday}}(t)} - c_{\text{trend}}(t) \tag{1}$$

The anomaly normalized infrastructure demand $\mathcal{D}$, a function of time t (daily resolution), is calculated by dividing infrastructure demand D (shown in Figure 2a) by weekday pattern D_{weekday} (shown in Figure 2b) and then subtracting the long-term trend c_{trend} (shown in Figure 2d).

[1]Estimates based on data from Watson (2022); Short et al. (2015); Department for Business, Energy, and Industrial Strategy (2022)

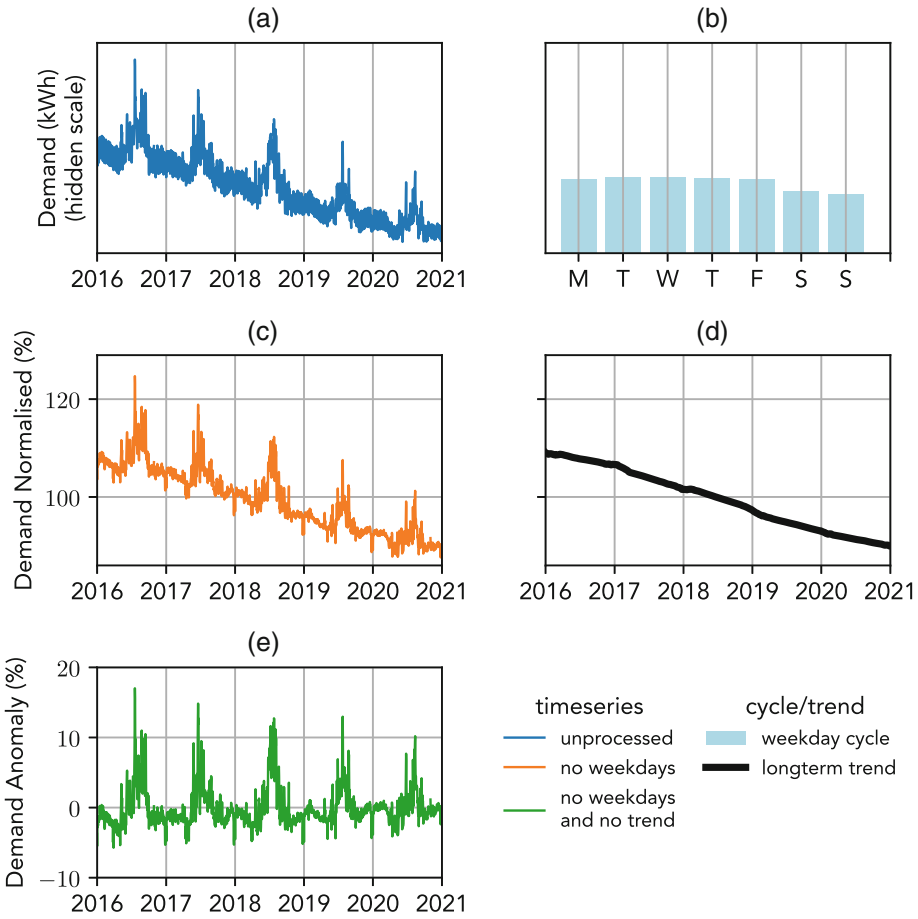

FIGURE 2 Processing steps for BT metered infrastructure demand, depicted for national data. Steps are reproduced at a regional level. Panels show: (a) Quality controlled data D. (b) Weekday pattern D_{weekday} is identified from a. (c) Normalized infrastructure demand (the result of dividing out b from a). (d) Long-term trend c_{trend} is identified from c. (e) Anomaly normalized infrastructure demand (longterm trend d is subtracted from c) uses the symbol $\mathcal{D}$ and forms the basis for analysing the infrastructure demand response to temperature.

Sensitivity tests showed that static values for D_{weekday} (as opposed to seasonally or annually evolving values) were sufficient in capturing day-of-the-week fluctuations in infrastructure demand.

Longterm infrastructure demand trend c_{trend}, calculated as the 1-year centred window running mean, is believed to result from operational energy efficiency improvements. In most regions, c_{trend} evolves gradually and continuously. Three out of the 14 regions contain discontinuous changes related to faster energy efficiency improvements.

2.2 | Temperature

The MERRA2 global weather reanalysis (Gelaro et al., 2017) is used as a source for temperature timeseries.[2] Daily gridded 2 m air temperature data is converted into regional timeseries by averaging over a latitude-longitude box for each distribution network operator zone (Figure 3). The resulting regional temperature data, T, is used in model fitting (2016–2020) and later as input to simulated infrastructure demand (1979–2020).

2.3 | GB-aggregated grid demand-net-wind

The transmission system operator controls the transport of electricity on the wider electricity network, and in GB is served by *National Grid ESO*. From Bloomfield et al. (2016, 2020a), we use reanalysis-derived grid demand and wind power. The demand–supply impact of weather and climate on the power system is the electricity grid demand minus wind power generation. These nationally aggregated daily variables are implemented with a single model realization, derived from MERRA2 data spanning 1979–2017, and without weekday varying component or residual noise. An analogous approach is taken in modelling weather-driven infrastructure electricity consumption in Section 3. We assume an installed wind power capacity of 24.5 GW in 2020 (Spry, 2023).

[2]Daily temperature timeseries for the gridboxes defined in Figure 3 are not sensitive to the choice of reanalysis. For example, ERA5 and MERRA2 outputs are highly correlated. However, a model incorporating additional meteorological variables (for example windspeed, precipitation) may require further consideration on the choice of reanalysis product.

3 | WEATHER-DRIVEN MODEL OF INFRASTRUCTURE ELECTRICITY DEMAND

Figure 4 shows the metered infrastructure demand to temperature response. Panel a presents the typical pattern seen in most BT regions: warmer temperatures increase infrastructure demand above a threshold (approximately 10°C), consistent with the need for cooling equipment dominating BT's overall energy usage nationally. In panel b, the region displayed (London) shows a particularly strong cooling response and no detectable heating response. In one region, Northern Scotland, there is a markedly contrasting behaviour with cooler temperatures (below 10.2°C) and differences in infrastructure temperature-sensitivity causing increased infrastructure demand, consistent with the dominance of office heating in energy usage. Elsewhere, the HDD effect is of much less significance than the CDD effect, but in most regions has at least a measurable impact. In all cases, it is noted that there is some spread in the temperature-demand relationship, indicative of other factors impacting infrastructure demand (and explored further in Section 4).

Infrastructure electricity demand is modelled with Heating and Cooling Degree Days (Taylor & Buizza, 2003). Our degree day functions take input of regional daily timeseries of temperature ($T(t)$) and are defined in Equation 2:

$$\mathrm{HDD}(T) = \begin{cases} T_{\mathrm{HDD}} - T & \text{if } T < T_{\mathrm{HDD}} \\ 0 & \text{otherwise} \end{cases}$$
$$\mathrm{CDD}(T) = \begin{cases} T - T_{\mathrm{CDD}} & \text{if } T > T_{\mathrm{CDD}} \\ 0 & \text{otherwise} \end{cases} \quad (2)$$

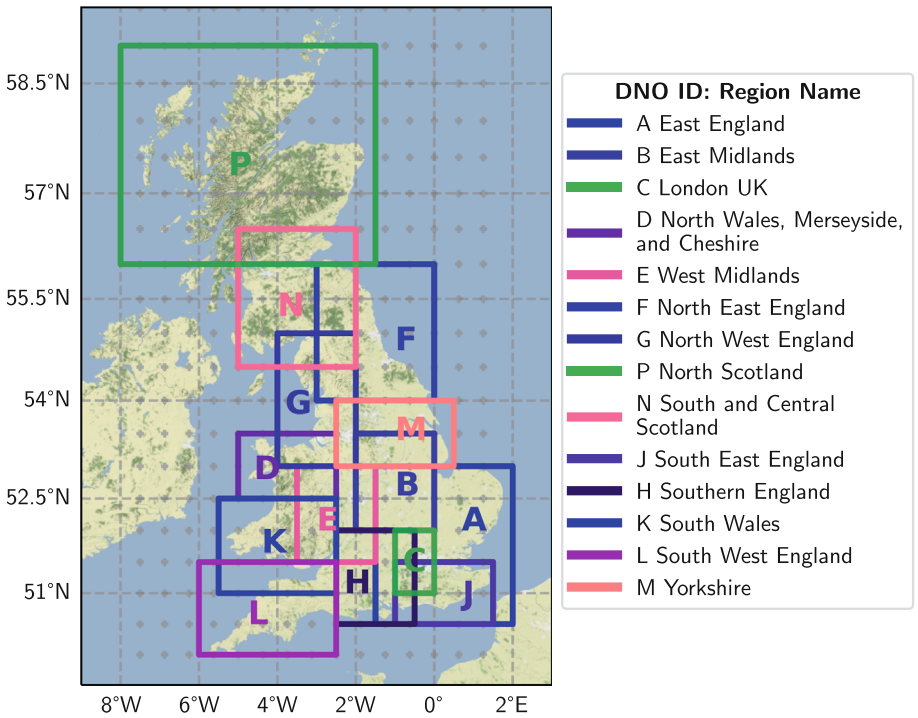

FIGURE 3 Gridboxes used to extract Temperature (2 m) from MERRA2, for the 14 Distribution Network Operator zones. Re-analysis gridpoints are displayed as dots, with 0.50 × 0.625 spacing (latitude × longitude resolution). Zone averages of temperature are calculated by weighting by the square of land-sea fraction for intersecting grid-points. Boundary co-ordinates are given in supporting information Table S1.

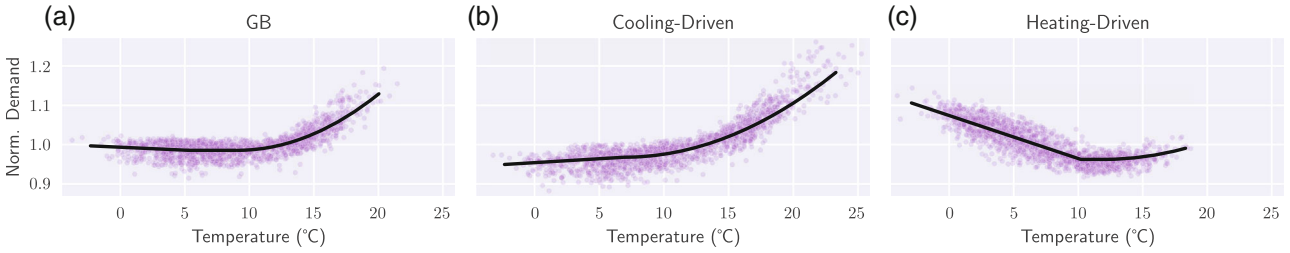

FIGURE 4 BT daily metered infrastructure demand (reconstructed to 2020 trend), in the three case study regions: GB, Cooling-Driven (London) and Heating-Driven (North Scotland). Values are normalized to remove weekday effects. Black curves indicate deterministic model fit.

In each region, these functions are used in fitting a new model of $\mathcal{D}$ by ordinary least squares. In each case, we allow the model to select terms, which are up to quadratic in HDD and CDD, and we neglect terms, which are shown to be negligible (using stepwise regression). In each case, the optimal fit identified either matches the form of Equation 3, or in some cases this form was detected as one of multiple fits whose error metrics are consistent. For simplicity, we then impose all models to take the form of linear HDD and quadratic CDD:

$$\mathcal{D}(T) = \mathcal{D}_0 + \alpha_{\mathrm{HDD}} \times \mathrm{HDD}(T) + \alpha_{\mathrm{CDD}} \times \mathrm{CDD}(T)^2 \quad (3)$$

The degree day functions are as defined in Equation 2, and $\mathcal{D}(T)$ is the modelled infrastructure demand. Intercept $\mathcal{D}$ and co-efficients for the three different regional models studied in detail given in Table 1.

Three regions are selected to represent distinct temperature-demand sensitives. Whilst 'North Scotland' has a strict geographical significance for BT (i.e., the data has a correspondence to real infrastructure installed across that region), the characteristic behaviour may be entirely relevant for a completely different type of infrastructure installed elsewhere, which could be, for example, a hospital in South Wales, or an office in North England, depending on the temperature-demand relation present. The three 'regions' are chosen to give as wide a representation as possible of different behaviours of infrastructure electricity consumption. Henceforth, to make it clear that these case studies should be considered for their specific temperature-demand behaviours, we refer to the regions as 'Cooling-Driven' (London), 'Heating-Driven' (North Scotland), and 'GB' (the sum total over subregions, reflecting a combination of heating and cooling behaviours, with behaviour broadly representative of other subregions).

Parameter uncertainty ranges are calculated by a random bootstrap sampling of daily infrastructure demand. The variation in temperature thresholds (T_{HDD} and T_{CDD}) calculated from sampling is below 1°C, whilst gradient parameters vary by less than 10% of their respective mean values.[3]

[3]Bootstrap sampling was conducted by creating new 5-year timeseries based on the grid demand data 2016–2020, and randomly re-sampling the years. A bootstrap size of 41 was used. Further tests limiting the data to a 3-year window at the start/end (ie. 2016–2018 and 2018–2020) showed parameters consistent and within the uncertainty range of the full 5-year version, indicating that despite long term trends in the mean energy use, the weather sensitivity was consistent.

4 | STOCHASTIC WEATHER-DRIVEN MODEL OF INFRASTRUCTURE ELECTRICITY DEMAND

The models introduced in Section 3 are deterministic, that is, for a known set of weather conditions, there is a singular estimate of the infrastructure demand $\mathcal{D}$. As noted in Section 3, there is a spread in the temperature-demand relationship. The output from the deterministic model can be interpreted as the expected $\mathcal{D}$ for a given set of weather conditions. The actual $\mathcal{D}$ which would be recorded on such a day may be either higher or lower than this expected value due to 'other factors' which are not being expressly modelled. In some cases such factors may be weather related—for example, additional variables such as humidity or wind speed—or from non-weather-related sources. However, no additional meteorological- or calendar-related impacts were detected in the BT consumption dataset.

The reduced variability in (deterministic) modelled $\mathcal{D}$ alters the probability distribution of demand, especially significant near the extreme tails. In the context of estimating reserve requirements it is therefore useful to represent the effect of these 'other factors' stochastically. We introduce a first-order autoregressive stochastic term, which encompasses the missing variability. A pseudo-random, normally distributed first-order autoregressive timeseries is constructed for the *residual* infrastructure demand component $\mathcal{D}_{\mathrm{res}}$ (i.e., the difference between modelled infrastructure demand and observed (metered) infrastructure demand after removing the effects of long-term trends). The calculation of this daily demand timeseries is shown in Equation 4:

$$\mathcal{D}_{\mathrm{res}}(t) = \rho_1 \mathcal{D}_{\mathrm{res}}(t-1) + Z(t) \quad (4)$$

$\mathcal{D}_{\mathrm{res}}(t)$, the residual infrastructure demand at step t is related to the previous time step multiplied by residual lag first-order autocorrelation ρ_1. The timeseries is initialized at $\mathcal{D}_{\mathrm{res}}(0) = Z(0)$. The normally distributed random component Z has mean 0 and standard deviation σ_Z related to the standard deviation of the infrastructure demand residual (Chatfield, 2003) and given in Equation 5:

$$\sigma_Z = \sqrt{1-\rho_1^2} \times \sigma_{\mathrm{res}} \quad (5)$$

The residual standard deviation σ_{res} introduces variability equivalent to that of observations minus model (but accounting for long-term trend).

Stochastic realizations are obtained by combining the deterministic and residual stochastic components, described in Equation 6:

$$\mathcal{D}^{(r)}(t) = \mathcal{D}(T(t)) + \mathcal{D}^{(r)}_{\text{res}}(t) \tag{6}$$

Each stochastic realization r of modelled demand $\mathcal{D}(t)$ corresponds to a different random sampling of the normally distributed term Z in Equation 4. The modelling of the stochastic noise term as normally distributed and lag 1 is justified in the supporting information in Figures S2–S4. Infrastructure demand $D(t)$ in physical units (kWh) is obtained by applying the inverse of Equation 1 to each realization $\mathcal{D}^{(r)}$ with some minor modifications:

$$D^{(r)}(t) = \left(\mathcal{D}^{(r)}(t) + c_{\text{trend}}(t_{2020})\right) \times D^{*}_{\text{weekday}}(t) \tag{7}$$

Instead of re-applying the original trend $c(t)$ (which only spans 2016–2020), we apply the static trend coefficient $c_{\text{trend}}(t_{2020})$ evaluated for mid-2020 (1st July) so that the modelled infrastructure demand is relevant to the most recent estimate of infrastructure energy efficiency. Additionally, the stochastic model cycles through different possible combinations of the weekday pattern coinciding on calendar dates: $D^{*}_{\text{weekday}}(t) = D_{\text{weekday}}(t + (r \bmod 7))$, the modulo offsets the weekday pattern of the realization by a constant number of days ranging 0 to 6, specific to realization number r. This ensures that the (non-meteorological) weekday effect is not unfairly suppressing/amplifying particular weather events that happen to overlap particular days of the week.

The distribution of daily infrastructure demand is shown in Figure 5. Histograms are calculated: 41×7 years of daily infrastructure demand deterministic model (from 41 years of MERRA2 data and seven implementations of the weekday cycle); 1750 realizations of the stochastic model (250 of each weekday offset); and 5 years of metered data (reconstructed to remove the underlying

TABLE 1 Degree day threshold parameters (°C). The thresholds determine the extent of the *heating* and *cooling* degree day domains.

Region	T_{HDD} °C	T_{CDD} °C	$\mathcal{D}_0$%	α_{HDD}%°C^{-1}	α_{CDD}%C^{-2}
GB	5.3	9.1	−1.58	0.15	0.12
Cooling-driven	6.9	6.9	−3.36	−0.2	0.08
Heating-driven	10.2	11.95	−3.91	1.1	0.07

Note: The infrastructure demand when not in either heating or cooling regime has value $\mathcal{D}_0$ (%). The heating and cooling responses are further characterized by gradients, α_{HDD}, α_{CDD}, measured in units, %°C^{-1} and %°C^{-2} respectively. Regions shown are GB, Heating-Driven (North Scotland) and Cooling-Driven (London), as in Figure 4, and a complete dataset covering all regions is given in supporting information Section 2, Figure S1 and Table S2.

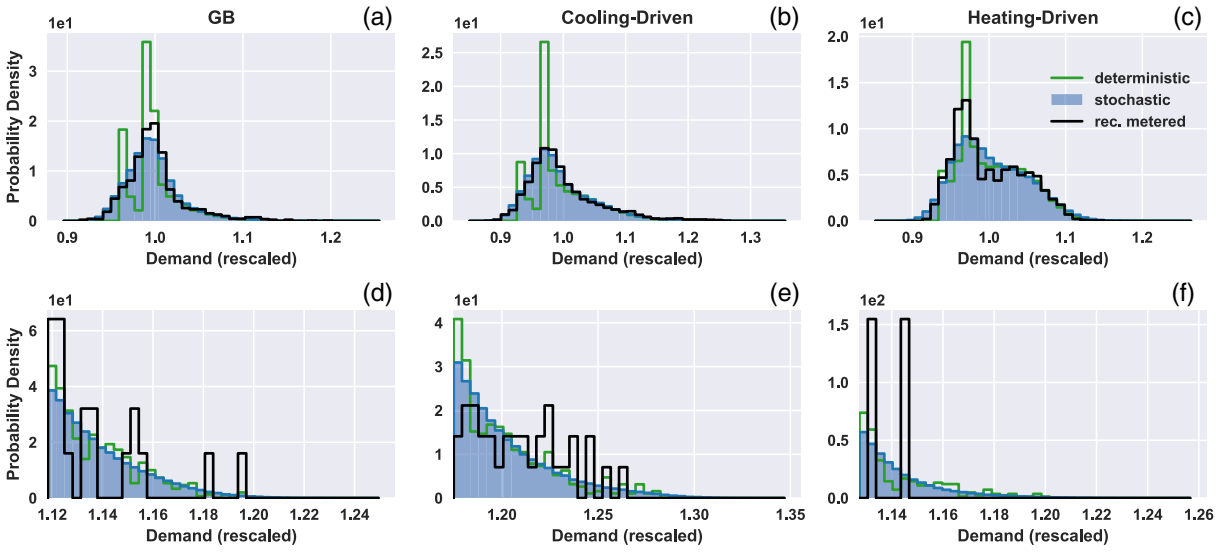

FIGURE 5 Probability distributions of Infrastructure Demand $\mathcal{D}(T)$ in rescaled units, full distribution (a–c) and top 1% of distribution (d–f). The *reconstructed* metered infrastructure demand is the original metered infrastructure demand rescaled to 2020 (applying a correction for removing the long-term trend c_{trend} by applying Equation 1, and then converting back into physical units with a static trend coefficient in Equation 7, with $r = 0$ for real calendar days). Scale is hidden in order to protect proprietary information of BT's infrastructure demand data.

long term trend). The probability distribution of the deterministic model is a poor match for the metered data, with two large spikes (corresponding to week-day and weekend infrastructure demand) and unrealistic lower distribution bound cutoff (if the temperature is such that there is no degree day induced demand, and it occurs on a Sunday, then the demand cannot be reduced any further). The stochastic model, however, re-introduces missing variability and provides a very accurate distribution fit for the GB/cooling-driven regions in particular. Whilst the metered data only samples five weather years, the stochastic model has thousands of realizations of 41 weather years, and is therefore a more representative weather-driven infrastructure demand distribution.

Figure 5 panels d–f show that, encouragingly, the right-hand tails of the stochastic models closely match the reconstructed infrastructure demand. The increased sample sizes of the stochastic models yield smoother probability distribution tail-ends than the metered infrastructure demand.

Extreme values are limited by the adopted normal distribution (probability of extreme values of demand are distributed $\sim e^{-D^2}$) and further by first-order correlation of the residual stochastic component (Equation 4). This model, with a large number of realizations ($n = 1750$) and spanning 41 years of weather input, should act as the most complete and accurate dataset from which we can derive estimates of possible infrastructure demand events and implications to reserve power infrastructure.

5 | RESULTS

5.1 | Infrastructure demand climatology

Figure 6 shows the 41-year climatology of modelled stochastic infrastructure demand, in each of the three regions. Additionally, the grid electricity demand-net-wind (deterministic model) is shown in panel d; 'demand-net-wind' is the shortfall of electricity load to be met by

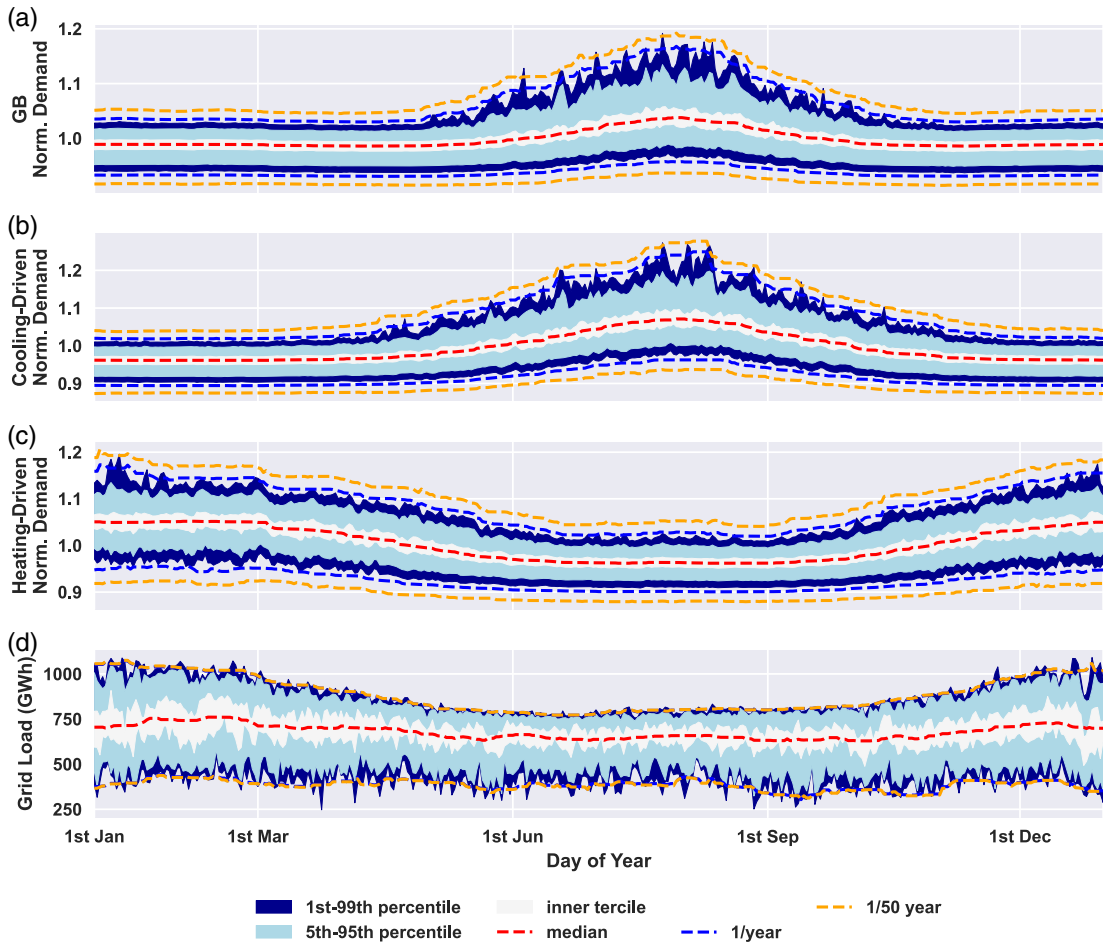

FIGURE 6 Climatology of daily infrastructure demand of GB, Heating-Driven (North Scotland) and Cooling-Driven (London) BT regions and of the grid demand-net-wind (Bloomfield et al., 2020a). Shaded areas are raw daily-climatology percentiles (sampling 41 weather years and 1750 stochastic realizations for BT infrastructure demand). Dashed lines use 15-day rolling median smoothing.

generation after subtracting the wind power generation, calculated by Bloomfield et al. (2020a). We do not explicitly model solar power, which is partially embedded in the grid demand model.

The Heating-Driven region has similar characteristics to the grid demand-net-wind, peaking in winter (cold weather) and suppressed weather-driven variability and low overall demand in summer. Conversely, GB and Cooling-Driven infrastructure demand variability and peaking are most significant in summer months. Given the significant seasonal variation in infrastructure demand, we can also expect to see seasonal variation in the 5-day (or N-day) energy consumption and hence the level of reserve capacity that must be available.

5.2 | Reserve capacity & seasonal variation

For critical reserve power infrastructure subject to strict operational time commitments (N-day reserve power), the installation capacity is determined by a small number of infrastructure high-demand events. Simply selecting the highest N-day energy consumption event observed in the original metered infrastructure demand data as a reference for the necessary reserve capacity is precarious since the dataset is limited and unlikely to reflect the most extreme values that could be expected if a longer baseline period was made available. Choosing the highest N-day energy consumption event from the simulated infrastructure demand (Sections 3 and 4) is an improvement, exposing the data to decades of weather events as well as many different realizations of the 'stochastic' component, ensuring a wide range of plausible outcomes for the combined effects of meteorological and non-meteorological impacts are explored. However, in this latter case, the value of the greatest N-day energy consumption is limited by the number of stochastic realizations, and since the model uses (unbounded) normally distributed noise, there is no upper bound to what the highest N-day energy consumption could be.

Therefore, in order to make a planning decision based on full use of the available weather information, but without arbitrary factors related to the model implementation, we must frame the problem in terms of a risk of exceeding the installed reserve capacity E.

We introduce indicator function $X(t_i)$ to describe whether the infrastructure demand accumulated over N-days (from time t_i to t_{i+N-1}) could have theoretically been supplied (0) or is exceeded (1) if reserve power had been relied upon:

$$X(t_i) = \begin{cases} 1 & \text{if } \sum_{j=0}^{N-1}\left(D_{i+j}\right) > E \\ 0 & \text{otherwise} \end{cases} \tag{8}$$

The statement $\sum_{j=0}^{N-1}\left(D_{i+j}\right) > E$ yields true if the N-day infrastructure electricity consumption exceeds the installed reserve capacity E. For convenience, we denote exceedance indicator $X(t_i)$ for a given year y of a given stochastic realization r as $X_{y,r}(t_d)$ where t_d is the corresponding day of the year. With no prior information about the infrastructure demand levels, the likelihood $\mathbb{P}_X$ that in a given year, the N-day energy consumption will exceed the reserve capacity E on one or more occasions is as follows:

$$\mathbb{P}_X = \frac{1}{N_y N_r}\sum_{y=1}^{N_y}\sum_{r=1}^{N_r}\left(1-\prod_{d=1}^{N_d}\left(1-X_{y,r}(t_d)\right)\right) \tag{9}$$

The probability of exceedance $\mathbb{P}_X$ is defined by averaging over years and realizations the complement to $\prod_{d=1}^{N_d}\left(1-X_{y,r}(t_d)\right)$ (i.e., the complement to no exceedance events occuring). Subscript r denotes a unique stochastic realization and y the calendar year (from 1979 to 2020) for the exceedance indicator X. The limits N_y, N_r, N_d are the number of years, realizations, and days in a year, respectively. The open script font for $\mathbb{P}_X$ emphasizes that it is the probability of one or more instances over a period of time N_d where $X(t_i) = 1$.

The relation between $\mathbb{P}_X$ and E is demonstrated in Figure 7, for the three case study regions, with the reserve commitment of $N = 5$. In the normalized units, 1 unit of energy equals the mean daily infrastructure demand, hence 5 units are equal to 5 average days of consumption, and so forth. In addition to the full-year case (black dashed line), we plot lines corresponding to meteorological seasons. In these cases, Equation 9 is revised, so that time indexes 1 to N_d correspond to the respective season.

As risk aversion is relaxed, the installed reserve capacity is reduced whilst the probability of exceedance $\mathbb{P}_X$ increases. For risk-averse behaviour approaching $\mathbb{P}_X = 0$, steeper gradients indicate an increasing cost for more marginal gains in risk reduction. The GB and Cooling-Driven regions experience the maximum energy-consumption events in late July/early August (consecutive days in the upper percentiles of Figure 6), hence, the relation between probability of exceedance $\mathbb{P}_X$ and installed capacity E is the same in a given year as it is for a given JJA (shown by the two respective curves matching in Figure 7). In the Heating-Driven region, it is DJF that closely matches the full-year relation. Demand-inducing low-temperature extremes spread beyond just DJF

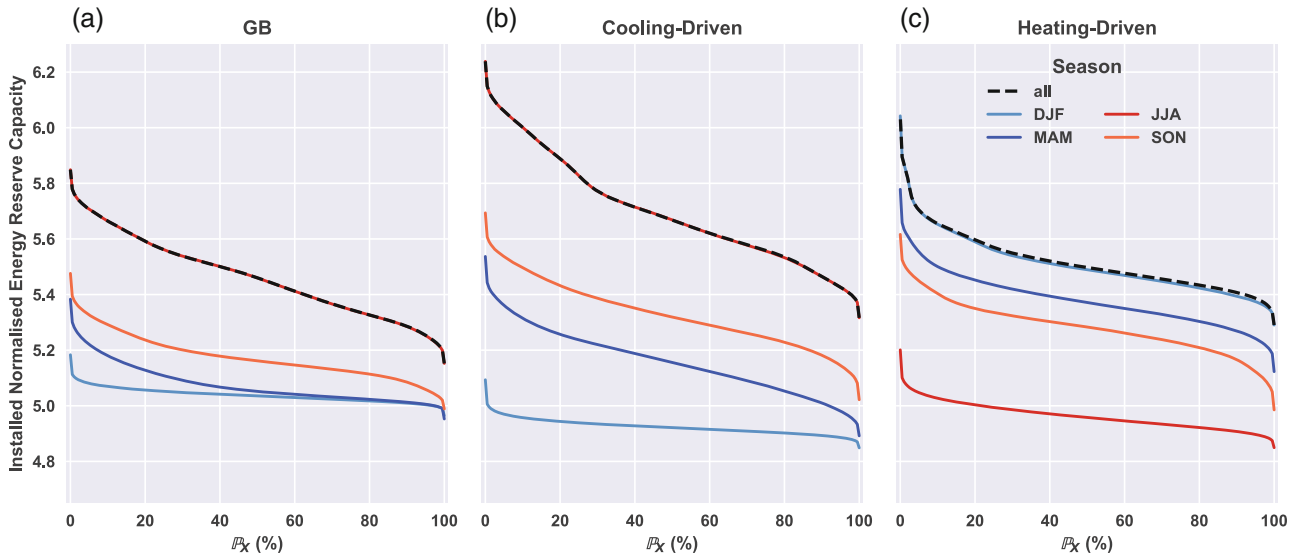

FIGURE 7 Capacity-exceedance relation (see Equation 9) shows the probability that N-day energy consumption exceeds reserve capacity at least once in a given season/year, in the case $N = 5$. Dashed line shows the full-year, whilst other lines correspond to meteorological seasons: December–February (DJF), March–May (MAM), June–August (JJA) and September–November (SON). In the normalized units (y-axis), 1 unit of energy is equal to the mean daily infrastructure demand.

(see Figure 6 Heating-Driven region), so the full-year curve sits slightly above the DJF curve.

An interpretation of the risk framework for BT's GB region using Figure 7, a reserve capacity (given on y-axis) of 5.56 normalized units has 25% probability $\mathbb{P}_X$ (given on x-axis) of energy consumption exceeding levels that could be supplied by the installed reserve capacity in a given year. Increasing the installed reserve capacity by 2.6% (to 5.71, slightly higher on the y-axis) reduces the exceedance probability to below 0.5% requires an additional 1.2% to 2.5% reserve capacity (5.78 to 5.85 units). Off-peak seasons have significantly reduced capacity requirements (corresponding to the overall lower infrastructure demand levels and variability, see Figure 6). There is a sizable minimum amount of *surplus* capacity that can be assumed to be available with near-certainty during these off-peak seasons, calculated from the gap between the full-year curve and off-peak season curve.

5.3 | Reserve-exceedance coincidence

The hazard faced by operators is not just risk of exceedance but the combination of reserve power being required at the same time. This hazard is sensitive to the total variability in energy consumption and the installed reserve capacity. To optimize managing the cost of hazard avoidance, the operator may in practice tolerate higher values of $\mathbb{P}_X$, if relying on a low probability of needing N-days of reserve.

This tradeoff can be formulated in terms of the underlying probabilities. First, we introduce indicator function $R(t_i)$, showing when reserve capacity is required for a full N day period starting at day t_i:t

$$R(t_i) = \begin{cases} 1 & \text{if reserve required } t_i \text{ to } t_{i+N-1} \\ 0 & \text{otherwise} \end{cases} \tag{10}$$

The likelihood of requiring reserve power for N days from a given start day is constant probability $P_R = \mathbb{P}(R(t_i) = 1)$. Each model realization has a unique corresponding realization of timeseries $R(t_i)$ and the value of P_R may be adjusted to reflect plausible prevalence. The assumption made of constant P_R is unrealistic, as P_R is likely to have seasonal variability and its own weather sensitivity, however, modelling a time-dependency for P_R is beyond the scope of our calculations.

The *coincidence* indicator $C(t_i)$ is introduced to mark the hazard of having both reserve requirement $R(t_i)$ and reserve exceedance $X(t_i)$:

$$C(t_i) = R(t_i) \cdot X(t_i) \tag{11}$$

The hazard probability in a given year without prior knowledge is calculated analogously to Equation 9:

$$\mathbb{P}_C = \frac{1}{N_y N_r} \sum_{y=1}^{N_y} \sum_{r=1}^{N_r} \left(1 - \prod_{d=1}^{N_d} \left(1 - C_{y,r}(t_d) \right) \right) \tag{12}$$

The probability of coincidence $\mathbb{P}_C$ is defined by averaging the complement to $\prod_{d=1}^{N_d}(1 - C_{y,r}(t_d))$ (i.e., the complement to no coincidence events occuring) over timeseries years and realizations. Similar to Figure 7, but instead demonstrating the capacity-coincidence relation, Figure 8 demonstrates how changes in the likelihood (P_R) of a full 5-day reserve event relates the installed reserve capacity to the probability of a coincidence failure.

Most decision-makers will focus on the left side of the plot, where $\mathbb{P}_C$ is low; here, the gradient is strongly impacted by changes to P_R. Being more risk-tolerant (i.e., willing to accept a higher chance $\mathbb{P}_C$ of failure) greatly reduces the reserve requirement, particularly when there is only a small chance (P_R) of needing to draw on the reserve.

Figure 8 shows that when taking into account the finite probability of the reserve capacity actually being needed (in addition to the infrastructure demand exceeding the installed capacity), less reserve capacity is needed for a given hazard threshold. The figure also shows the obvious result that a decision-maker assuming lower risk of $R = 1$ has a lower requirement for installed reserve capacity.

However, in the extreme case where the installed capacity is so low as to never meet a full N-days requirement, risk management policy is essentially a bet on the occurrence of $R = 1$. This lower-limit on the installed capacity corresponds to lines in Figure 8 where the $\mathbb{P}_C$—Capacity relation drops off, becoming a vertical line below that point and this occurs at a $\mathbb{P}_C$ value equal to the probability of reserve, integrated over the year, that is, $1 - (1 - P_R)^{365}$. This is visible in Figure 8 panel a (GB), but too low to be visible in panels b, c.

The Cooling-Driven region again has the highest capacity requirements due to the greater CDD sensitivity, resulting in higher energy consumption during the most extreme events. The Heating-Driven region (which experiences both heating, and to a lesser extent cooling, behaviour) has the steepest gradients, owing to the greater total variability of energy consumption across the full-year (compared to GB and Cooling-Driven where weather-driven variability occurs from exposure to high temperatures primarily in summer months).

5.4 | Surplus variability

As discussed previously (Figure 6), there is a clear seasonal and meteorological dependence of BT's infrastructure electricity demand, and hence the energy required to meet their 5-day reserve requirement varies similarly (Figures 7 and 8). Consistent with this, if the installed capacity of the reserve remains constant throughout the year, there are periods where the full installed capacity is not required, referred to here as 'surplus'.

Having developed a framework for linking risk preference to the installed reserve capacity levels, we now seek

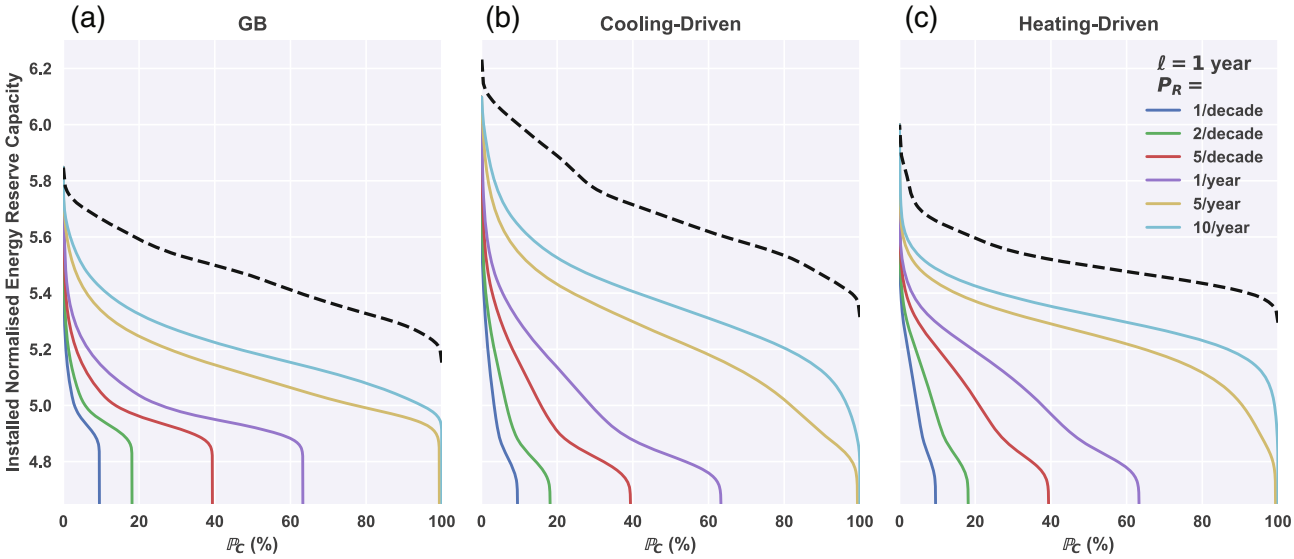

FIGURE 8 Capacity-coincidence hazard relation (see Equation 12). Figure shows the probability that N-day energy consumption ($N = 5$) will exceed the reserve capacity at the same time that N-day's reserve power is required, at least once in a given year. A range of reserve probability, P_R, defined in terms of likelihood of an N-day reserve requirement on any given day, results in adjusted capacity-coincidence curves. An increase in P_R is associated with increase in hazard risk $\mathbb{P}_C$. The dashed line represents hazard risk equal to exceedance risk, that is, $P_R = 100\%$ and therefore $\mathbb{P}_C = \mathbb{P}_X$. The normalized energy units are as previously described.

to quantify how much *surplus* capacity can be exploited for benefits beyond its use as a backup power source. This introduces an additional hazard: if too much surplus is used during a period of low infrastructure demand, there may not be sufficient stored energy for N-day reserve power operation during a subsequent period of higher infrastructure demand.

For a system with a likelihood P_R of having to use the reserve capacity for N-days from a given starting day, there is probability $1-(1-P_R)^{365}$ of one or more periods requiring N-day's reserve power in a given year. Consider, for example, a decision-maker operating a system with N-day reserve probability $P_R = 1/365$ on any given starting day, and whose risk preference is for up to 1% probability of at least one coincidence event in a given year (i.e., they are aiming for a 99% assurance of meeting reserve power commitments for an entire year). In the absence of any reserve power system present, the value $P_R = 1/365$ evaluates to a 63% likelihood of failure in a given year. However, this risk can be mitigated by installing a quantity of reserve power. In the example systems, installing 5.43, 5.66, 5.49 units of reserve power in the GB, Cooling-Driven and Heating-Driven regions, respectively, ensures that $\mathbb{P}_C < 1\%$ (likelihood of a coincidence event where reserve is both required and insufficient for N-day supply) is satisfied, a significant improvement over the 'natural' failure likelihood of 63% when $P_R = 1/365$.

Given that the installed capacity remains constant, the surplus capacity is calculated by subtracting N-day energy consumption from the installation capacities identified. The annual levels of safe seasonal surplus capacity resulting from the stochastic model are shown in Figure 9, as functions of day of the year.

In Figure 9, 'worst case' levels of surplus observed in the stochastic model on a given day of the year (or within 1 week either side) are depicted by the lower dashed curve. For some periods of the year, the 'worst case' levels of safe seasonal surplus still leave a significant baseline amount (shaded green). As long as the 41 years weather data and (1750 realizations of stochastic component) are representative of the full range of infrastructure demand levels that could be experienced, then these shaded green areas give a strong indication of safe levels of reserve almost guaranteed to be available even during the most extreme weather events historically observed for that time of year. Using surplus in excess of the 'safe' levels may sometimes be possible, but induces an additional exceedance hazard (i.e., the overall risk of the reserve not meeting 5-day commitments would be increased). Such operation would require skilful forecasts of infrastructure demand levels at least N-days ahead, to support decisions on how much surplus above safe levels can be utilized for non-reserve purposes.

Periods when the climatological surplus minima crosses below zero indicate that even if dedicating all capacity towards reserve power (setting the amount of surplus to zero), there is the possibility of not meeting the requirements for supplying sufficient reserve

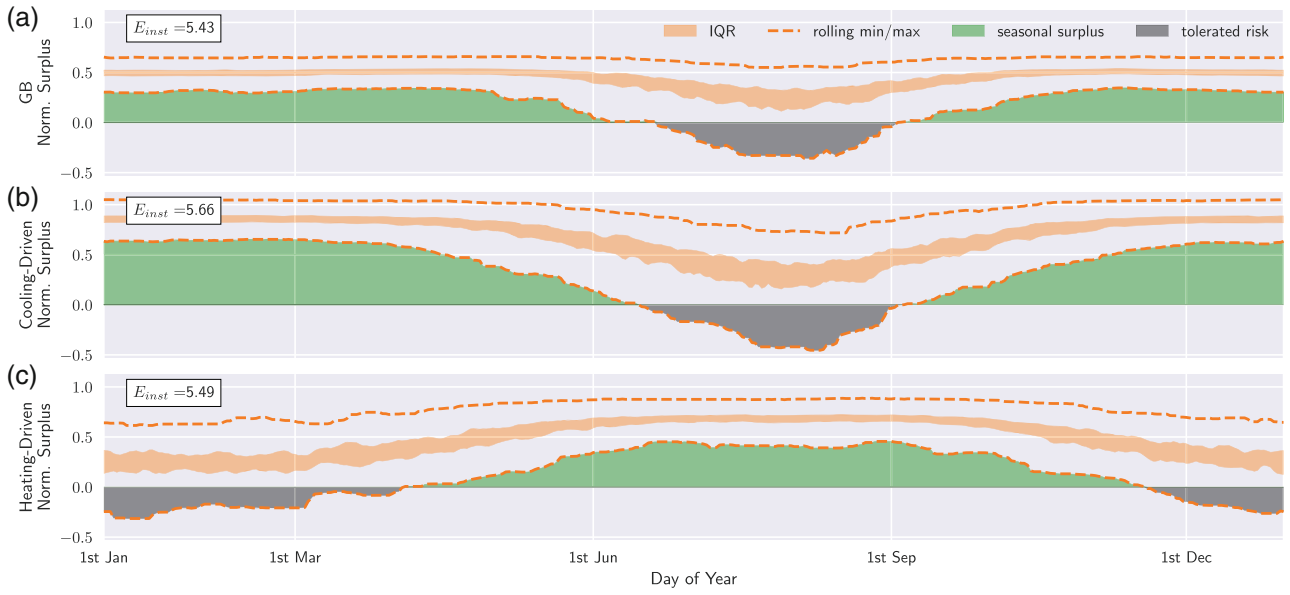

FIGURE 9 For three example systems, reserve capacity installation E_{inst} is set such that the probability $\mathbb{P}_C$ in a given year of failure to meet N-day delivery requirements whilst reserve is in use is 1. Green-shaded regions show levels of *surplus* capacity, and grey-shaded regions show tolerated risk concentrated in periods where infrastructure demand is highest. Orange shaded regions show the inter quartile range of N-day ahead surplus capacity. Dashed lines indicated a 15 day rolling window of the climatological minima and maxima (i.e., the highest value to occur on a given day of the year or during the neighbouring 7 days either side).

capacity. This *tolerated risk* is shaded grey. In this situation of energy consumption exceeding installed reserve, all capacity should be made available for reserve power operation.

5.5 | Surplus allocation relation to risk tolerance

Let us consider a decision-maker with access only to climatological information: only the historic weather and infrastructure demand data is known. The climatological decision-maker will base their choices of surplus allocation on the climatological worst-case (i.e., allocating the 'green' levels of surplus capacity shown in Figure 9).

We continue with the assumption of $P_R = 1/365$, but now explore a range of risk tolerances in addition to $\mathbb{P}_C = 1\%$.

Surplus accumulated annually for systems installed to meet a variety of different $\mathbb{P}_C$ values are shown in Figure 10a. Increasing $\mathbb{P}_C$ reduces the level of reserve capacity required, which therefore also reduces the annual surplus accumulation. In all three regions, increasing $\mathbb{P}_C$ results in a reduction to the accumulated surplus.

The Cooling-Driven region (with greatest temperature sensitivity) shows the highest levels of accumulated surplus capacity. At lower $\mathbb{P}_C$ values, the Heating-Driven region has the least opportunity in surplus capacity operation, although it does outperform GB at $\mathbb{P}_C = 5\%$; tolerated risk in the Heating-Driven region is spread out over a longer period, so an increase to $\mathbb{P}_C$ has comparatively lower impact on the installed capacity E. Most of the change in surplus served relates directly to shifting the green region vertically on the graph by some constant offset, it is only the interface between the surplus and exceedance periods (green and grey) that a minor non-linear contribution to surplus capacity further affects the results.

5.6 | Surplus allocation relation to forecast information

A decision-maker with a robust weather-driven model of infrastructure demand should be able to make quite accurate forecasts of the deterministic component, albeit limited to the skill of temperature forecasts up to 5-days ahead, and errors accumulated in model conversion from temperature to infrastructure demand.

Consider two further decision-makers. First, a decision-maker with access to a perfect forecast of the weather-driven infrastructure demand but no information about the stochastic component, which we label the *deterministic* decision-maker. Second, a decision-maker with perfect forecast knowledge of both weather-driven and stochastic infrastructure demand components, which we label the *perfect* decision-maker. In this theoretical excercise, these cases can show the potential value, in terms of increased surplus allocation, of using forecast information in the decision-making, and demonstrate the importance of sampling the residual variance in order to estimate upper-bounds to a perfect decision-maker.

In the case of perfect information, a decision-maker knows precisely how much surplus to allocate for the N-days ahead and will maximize the amount of surplus at no risk of exceedance. The deterministic decision-maker has to reduce their forecast allocation of surplus

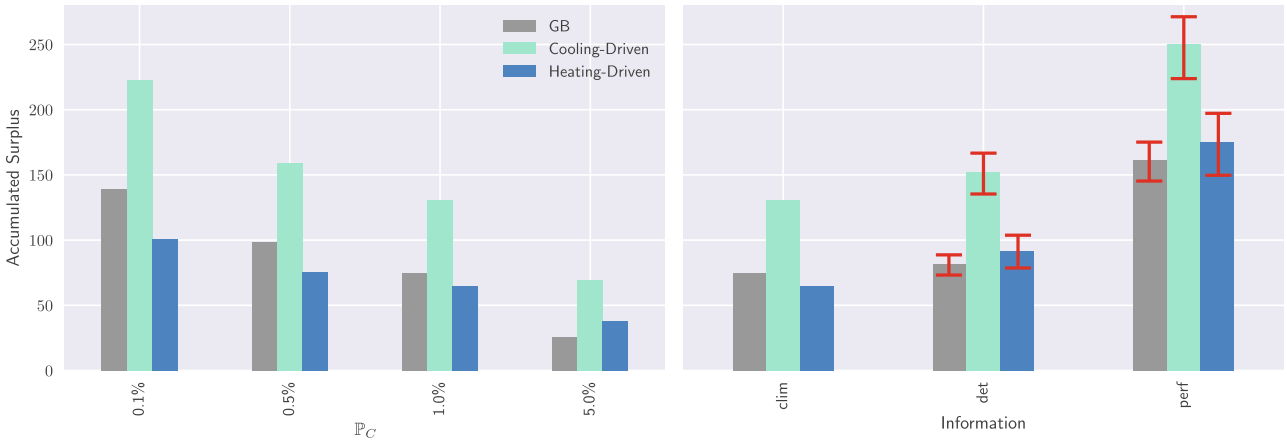

FIGURE 10 Accumulated surplus under different scenarios (for probability of N-day reserve needed $P_R = 1/365$, for $N = 5$). Left: Installed capacity values E (relating to specific coincidence probability tolerances $\mathbb{P}_C$) and resulting accumulated surplus (normalized units). Right: With $E(\mathbb{P}_C = 1\%)$, we explore surplus accumulated under three different decision-making scenarios. Error bars show the 5% to 95% range in outcomes across years and realizations.

by a constant offset value, matching the upper limit of stochastic-driven energy consumption. Theoretically, this is unbounded, however, we choose a finite value corresponding to 5σ deviation, so that there is almost no discernible increase in risk. In reality, perfect forecast information would not be possible, so this case presents an upper-bound of skill.

In Figure 10b, we see gains in the accumulated surplus when using better forecast information, with the perfect decision-maker benefiting the most. The approach outlined introduces little-to-no risk from increasing surplus operation above seasonally safe levels, demonstrating the potential value of forecast information. Sub-seasonal energy forecasts (derived from meteorological forecasts) may aid decision-makers to exploit this large potential value, by anticipating N-day demand (and hence surplus levels) 1–4 weeks ahead (Gonzalez et al., 2021; Goutham et al., 2022). These forecasts could, for example, allow participation in the futures markets, with the amount of surplus capacity traded on the market increased up to realtime as forecast skill improves at shorter lead times (Dorrington et al., 2020).

An approach for decision-making under this uncertainty could explore trade-offs of adopting a more risky operational strategy (allowing a small but finite probability of exceedance based on forecast information) in conjunction with a more risk-averse planning strategy (i.e., over-building reserve-capacity). This would more evenly distribute risk across the year, instead of concentrating risk around climatological infrastructure demand highs and the gains in surplus allocation could further offset building costs.

5.7 | Meteorological drivers of surplus and grid electricity load

BT's national 'GB' infrastructure demand peaks in summer due to the strong CDD effect, contrasting with the grid demand and demand-net-wind which have strong winter peaking. The Cooling-Driven region has a comparatively stronger CDD dependence and, in fact, no overall HDD effect (instead, the negative coupling coefficient acts to extend the cooling impact to lower temperature ranges). The Heating-Driven region is an outlier from other BT regions, instead acting more in line with the grid demand and demand-net-wind, with strong HDD coupling and a weak cooling effect. As the amount of installed wind power capacity is increased, the grid demand-net-wind is increasingly sensitive to wind, although HDD impacts still play an important role in explaining grid demand-net-wind in Britain (Boßmann & Staffell, 2015).

Having explored the potential role of surplus capacity in the different weather-driven systems (GB/Cooling-/Heating-Driven), we now seek an understanding of the wider electricity-network behaviour in relation to surplus allocation and whether the surplus is available at a time when the wider grid might need it. Using the Bloomfield et al. (2020a) dataset for grid demand-net-wind (MERRA2, spanning 1979–2017), we compare the deterministic components of the infrastructure *demand* to the wider network.

Grid demand-net-wind is characterized by strong temperature and wind sensitivity (Beerli & Grams, 2019; Bloomfield et al., 2020b). In winter, there is heightened weather-driven variability (large differences between a cold, low-wind day compared to a mild, windy day). In summer, it is on average lower, has a reduced weather-driven variability, and the distribution of demand-net-wind values is positively skewed. This seasonal difference is seen when comparing panel g in Figures 11 and 12. Marginal distributions of the three modelled systems' surplus capacity are shown in panels a—c, and the joint probability distributions in panels d—f.

In winter, the GB and Cooling-Driven regions are narrowly concentrated around a high surplus (towards 0.4 to 0.5 and 0.8 to 0.9, respectively). The Heating-Driven region surplus capacity has a weak negative correlation to grid demand-net-wind, although this value is not significant at $r = -0.33$.

In summer, the Heating-Driven region is narrowly concentrated at high surplus capacity (similar to the behaviour of GB and Cooling-Driven in the winter period). The grid demand-net-wind does not reach near the maximums experienced in winter (during cold, less-windy periods). There is no correlation between grid demand-net-wind and surplus capacity (R^2 is less than 0.02 in each region).

A reserve power system operating in a GB or Cooling-Driven regime has significant potential to provide balancing services to the wider electricity network. Figure 11 motivates making surplus available during winter periods, whilst Figure 9 shows this to be possible. These non-reserve purposes may involve storing energy during low demand-net-wind periods, and releasing energy during high demand-net-wind periods.

Figure 10 indicates that use of forecasts can increase the amount of surplus made available for non-reserve purposes in a given year. Skilful forecasts may also allow Heating-Driven type systems to intermittently provide surplus capacity during the winter period, however, there is no consistent safe level, and Figure 11 panel f shows some negative correlation, possibly indicating that the surplus is less likely to be available during high demand-net-wind periods.

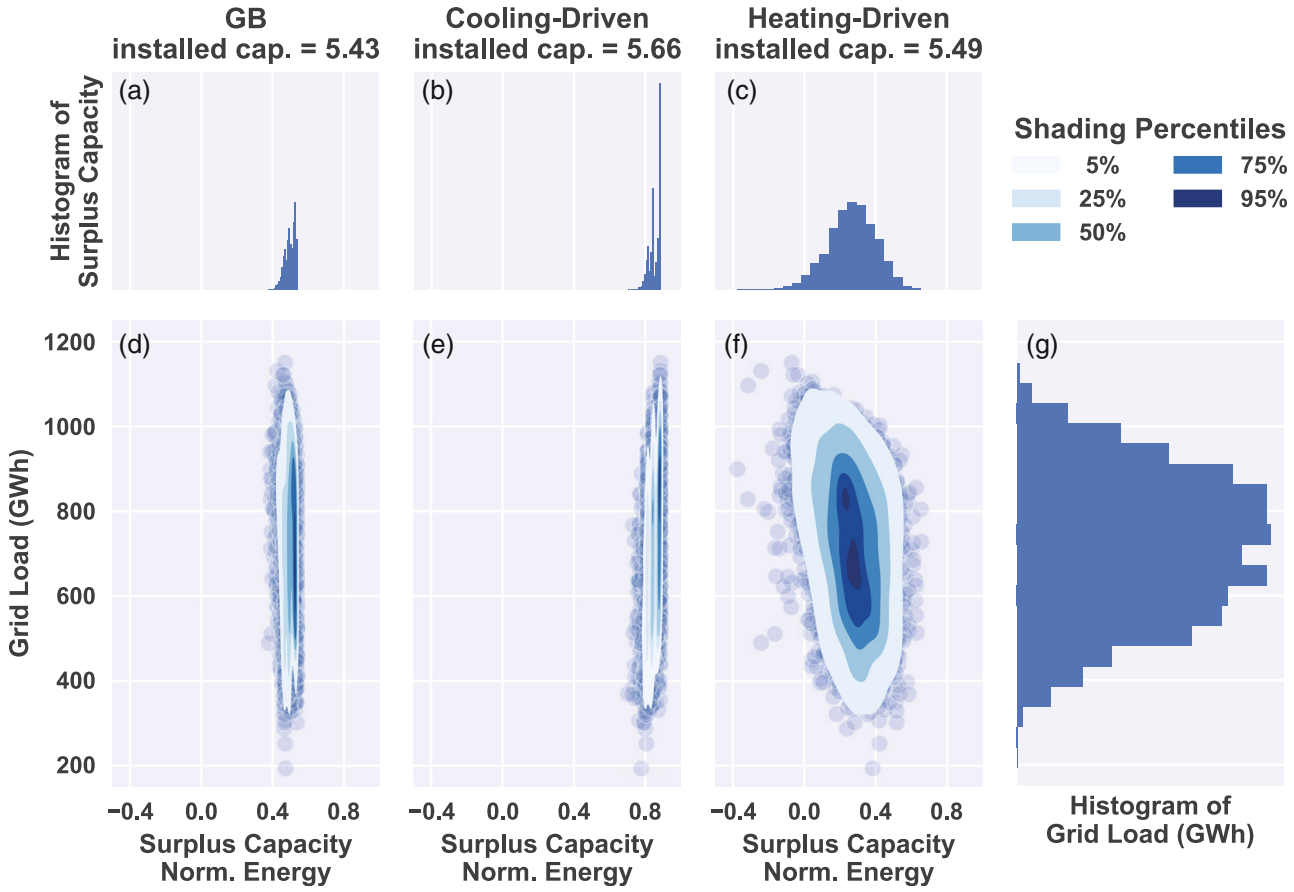

FIGURE 11 Bi-variate distributions (panels d–f) and respective marignal distributions (panels a–c and g) demonstrate how grid demand-net-wind (from Bloomfield et al. (2020a)) relates to infrastructure demand (GB, Cooling-Driven and Heating-Driven). Data is from the extended winter period (December–March).

6 | DISCUSSION

In any critical infrastructure, decision-makers will have a dialogue with industry regulators to discuss the cost-risk trade-offs and the extent to which some risks are considered unreasonable to mitigate. We have developed a framework for decision-makers to assess trade-off between installed reserve capacity and risk of failure, using a range of plausible values P_R for the probability of needing N-day reserve capacity, and a range of permissible hazard risks $\mathbb{P}_C$.

This framework makes some simplifying assumptions: we do not discuss the implications of longer (or shorter) periods of reserve power usage. In our case study, we made the assumption that P_R has no time-of-year dependency; it is more likely, however, that in reality, reserve capacity will be required in grid failures induced by extreme weather such as storms and heatwaves, both of which have a strong seasonal dependence. It is worth considering this context when analysing results: unless correlations between $R(t_i)$ and $X(t_i)$ are explicitly modelled, one should err towards choosing a more risk-averse value for reserve capacity to account for this simplification (or consider increasing the value of P_R to an upper bound).

For some critical infrastructure operators, past occurrences of operating N-day's reserve power may be rare or have never occurred; the event may be considered a *black swan* event, so P_R is unknown. In such cases, it is up to the decision-maker (and regulator) to agree upon appropriate quantities of reserve capacity to be installed, and the resulting exceedance probabilities.

Figure 10 shows the high potential value, in terms of surplus allocation, in using extended range forecasts in the decision-making. The theoretical upper limits, described by the deterministic (meteorological forecast only) decision-maker and so-called perfect decision-maker (correctly predicting the precise meteorological and noise impacts to infrastructure demand), are much higher than the baseline climatological yields. Assuming that the infrastructure temperature-demand relation is well modelled, forecast skill in predicting the deterministic component of infrastructure demand should be high in the week ahead, and measurable up to 4 weeks ahead,

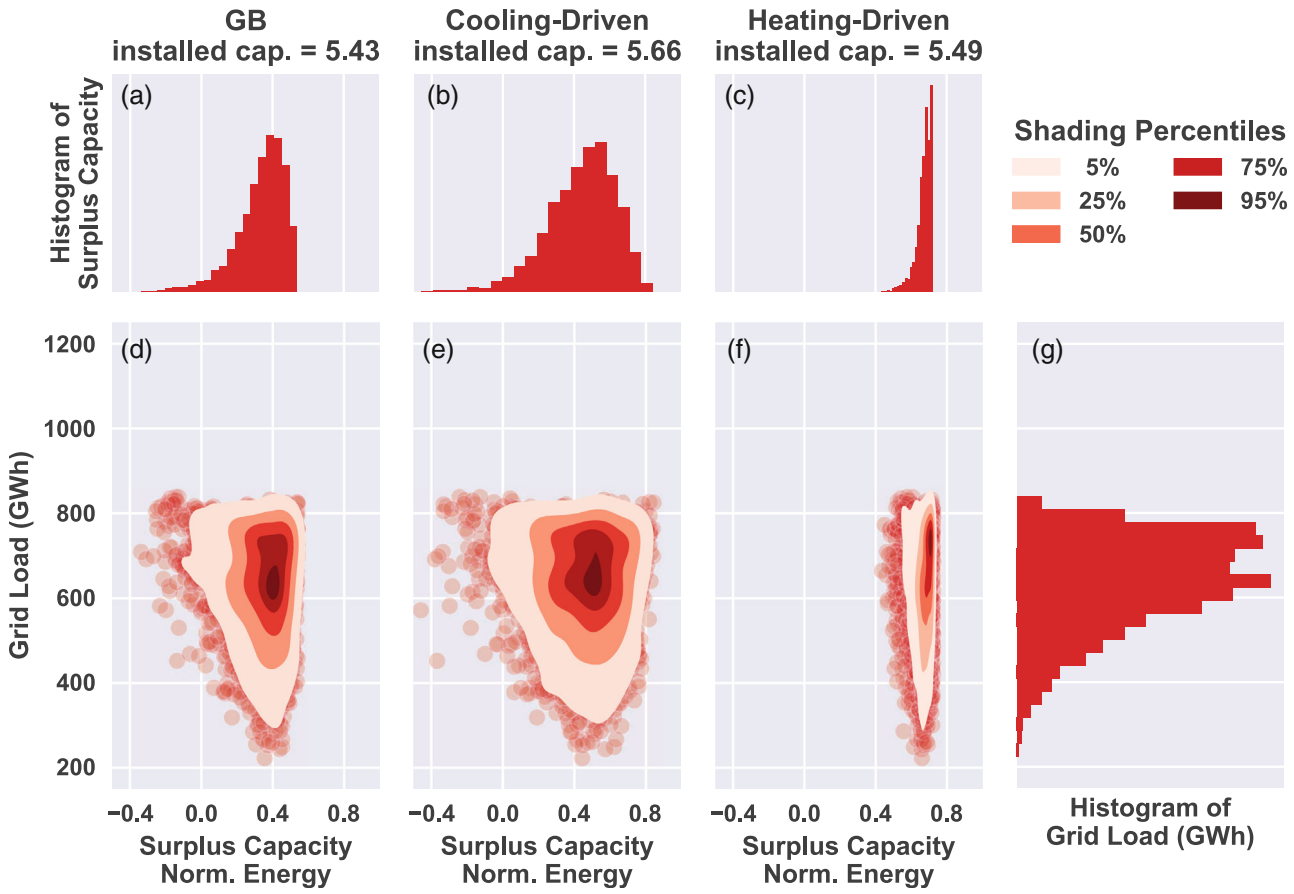

FIGURE 12 As in Figure 11, but showing the Extended Summer period (June–September).

allowing week-ahead allocation of surplus comparable to the theoretical 'deterministic' decision-maker. Any additional skill in predicting the stochastic component, for example through employment of an ARIMA model (Weisang & Awazu, 2008), could see surplus allocation between the bounds of 'deterministic' 'perfect' decision-makers. This theoretical exercise demonstrates the value to decision-making to allocate surplus using accurate forecasts, although as no 'perfect' forecast is possible this upper bound is higher than what may be achieved in reality.

Forecast lead times from day-ahead to extended range are relevant for applications in the energy sector and across industries (Bloomfield et al., 2021; Domeisen et al., 2022; White et al., 2017), with extended range allowing participation in trading ancillary service capacity weeks ahead, and shorter-range important for accurately knowing day and week ahead surplus availability. Forecasts can also be used to predict and warn of exceedance events. Decision-makers may benefit greatly from adopting a risk-tolerant approach, compensated by additional increases in reserve capacity, more evenly distributing risk across the year whilst increasing surplus annual accumulation.

There are multiple possible uses for surplus capacity, including ancillary services such as frequency balancing and peak-load shaving. The added value of surplus capacity can be captured with different metrics relevant to these different use cases.

7 | CONCLUSION

The transition to a low-carbon energy system offers challenges and opportunities for rethinking how we plan and use energy. In this paper, we explore the synergies between the need for clean 'backup' energy sources for critical infrastructure, and the potential for utilization of 'surplus' capacity in these resources in order to meet other energy needs (particularly ancillary services to the wider national power system).

Weather-driven models of infrastructure electricity demand, including a stochastic representation of residual uncertainty, were developed for three example critical infrastructure systems (based on BT regions). In each case, these models were used to estimate the size of the energy-reserve required to provide 5-day operational capacity in the event of regional power outage or black

swan events. The size of the store required is dependent on the risk tolerance of the critical infrastructure asset, and is linked to *coincidence risk*; the probability of both having a power system outage *and* having a 5-day infrastructure demand period which exceeds the total reserve capacity.

For the systems examined, a clear seasonal behaviour was observed (corresponding to energy-use driven primarily by heating, cooling, or a mixture of both). This clearly indicates that a reserve energy supply designed to meet 5-days of infrastructure demand during the peak season will have surplus capacity in the off-peak season. For cooling-dominated systems, which describes the bulk of the BT case study and approximately 0.5% to 1% of GB grid demand, the greatest surplus occurs at times of greatest value to the wider power system (i.e., during the winter when the need for generation capacity is greatest on the national power system as a whole).

The existence of clear seasonal variations in energy consumption provide a direct pathway to estimate the 'surplus' storage that can be further enhanced by meteorological forecasts. Use of skilful medium to extended range forecasts to identify infrastructure demand levels in advance (i.e., identify periods where the amount of surplus that can be released is greater than that which would be expected on a purely climatological basis alone), may prove highly valuable. For context, a simple test case with a *perfect* forecast doubled the available surplus.

The approaches outlined in this paper employ a weather reanalysis dataset in order to calculate weather- and seasonally-varying impacts to reserve power infrastructure planning and operation. A key observation in developing this analysis is the importance of including a stochastic representation of the residual uncertainty associated with the infrastructure demand. Failing to represent these processes lead to substantial errors in the size of capacity installed with respect to risk tolerance.

The comparison of decision-making under climatological, deterministic-only and *perfect* forecasts (including the stochastic component) suggest improvements in the amount of surplus that can be allocated. However, it should be emphasized that the weather in the reanalysis should not be considered fully representative of present and near-future events, with the sample range unable to fully explore decadal variations and current climate change impacts. Into the future, impacts of climate and ecological breakdown and industry response such as heat and transport electrification, will greatly affect weather-drivers of infrastructure demand and what is required from reserve systems, for example driving increased grid demand-net-wind load and variability in winter months (Bloomfield et al., 2016; Boßmann & Staffell, 2015; Peacock et al., 2023). Practical application of the approaches outlined should consider implementing climate impacts into modelling, alongside other projected system changes (such as reductions in the infrastructure temperature-demand sensitivity if more efficient equipment is installed in future).

AUTHOR CONTRIBUTIONS

James Fallon: Conceptualization (equal); formal analysis (lead); investigation (lead); methodology (equal); validation (lead); visualization (lead); writing – original draft (lead); writing – review and editing (equal). **David Brayshaw:** Conceptualization (equal); investigation (supporting); methodology (equal); supervision (lead); visualization (supporting); writing – original draft (supporting); writing – review and editing (equal). **John Methven:** Conceptualization (equal); investigation (supporting); methodology (equal); supervision (supporting); visualization (supporting); writing – original draft (supporting); writing – review and editing (equal). **Kjeld Jensen:** Conceptualization (equal); investigation (supporting); methodology (equal); resources (equal); supervision (supporting); writing – original draft (supporting); writing – review and editing (equal). **Louise Krug:** Conceptualization (equal); investigation (supporting); methodology (equal); resources (equal); supervision (supporting); writing – original draft (supporting); writing – review and editing (equal).

ACKNOWLEDGEMENTS

This work was conducted on a PhD studentship through the SCENARIO Doctoral Training Program, funded by NERC, and in a CASE partnership with BT. Thanks are given for all the help and support received from staff members at BT Research and University of Reading.

FUNDING INFORMATION

BT (British Telecommunications plc); Natural Environment Research Council (NERC), SCENARIO Doctoral Training Programme, Project Code: F4114908.

DATA AVAILABILITY STATEMENT

Temperature timeseries are derived from gridded MERRA2 weather reanalysis (Gelaro et al., 2017). MERRA2 products are accessible online through the NASA Goddard Earth Sciences Data Information Services Center (GES DISC). Weather-derived GB aggregate timeseries of demand and wind power are adapted from Bloomfield et al. (2020a) (available under CC BY 4.0 licencing). Infrastructure electricity demand datasets are kindly provided by BT PLC and are not made available online.

ORCID

James Fallon https://orcid.org/0000-0002-6321-7456
David Brayshaw https://orcid.org/0000-0002-3927-4362

REFERENCES

Beerli, R. & Grams, C.M. (2019. ISSN 0035–9009, 1477-870X) Stratospheric modulation of the large-scale circulation in the Atlantic–European region and its implications for surface weather events. *Quarterly Journal of the Royal Meteorological Society*, 145(725), 3732–3750. Available from: https://doi.org/10.1002/qj.3653

Bloomfield, H.C., Brayshaw, D.J., Shaffrey, L.C., Coker, P.J. & Thornton, H.E. (2016. ISSN 1748-9326) Quantifying the increasing sensitivity of power systems to climate variability. *Environmental Research Letters*, 11(12), 124025. Available from: https://doi.org/10.1088/1748-9326/11/12/124025

Bloomfield, H., Brayshaw, D. & Charlton-Perez, A. (2020a) MERRA2 derived time series of European country-aggregate electricity demand, wind power generation and solar power generation. https://doi.org/10.17864/1947.239

Bloomfield, H.C., Brayshaw, D.J. & Charlton-Perez, A.J. (2020b. ISSN 1350–4827, 1469–8080) Characterizing the winter meteorological drivers of the European electricity system using targeted circulation types. *Meteorological Applications*, 27(1), e1858. Available from: https://doi.org/10.1002/met.1858

Bloomfield, H.C., Brayshaw, D.J., Gonzalez, P.L.M. & Charlton-Perez, A. (2021. ISSN 1469-8080) Pattern-based conditioning enhances sub-seasonal prediction skill of European national energy variables. *Meteorological Applications*, 28(4), e2018. Available from: https://doi.org/10.1002/met.2018

Borzenko, V.I. & Dunikov, D.O. (2017. ISSN 1742–6588, 1742–6596) Feasibility analysis of a hydrogen backup power system for Russian telecom market. *Journal of Physics Conference Series*, 891, 012077. Available from: https://doi.org/10.1088/1742-6596/891/1/012077

Boßmann, T. & Staffell, I. (2015. ISSN 03605442) The shape of future electricity demand: exploring load curves in 2050s Germany and Britain. *Energy*, 90, 1317–1333. Available from: https://doi.org/10.1016/j.energy.2015.06.082

Chatfield, C. (2003) *The analysis of time series: an introduction*. New York: Chapman and hall/CRC.

Chawla, S., Kurani, S., Wren, S.M., Stewart, B., Burnham, G., Kushner, A. et al. (2018. ISSN 0022-4804) Electricity and generator availability in lmic hospitals: improving access to safe surgery. *Journal of Surgical Research*, 223, 136–141. Available from: https://doi.org/10.1016/j.jss.2017.10.016

CPNI. (2021) Critical National Infrastructure | Centre for the Protection of National Infrastructure.

Department for Business, Energy & Industrial Strategy. (2022) Historical electricity data: 1920 to 2021.

Domeisen, D.I.V., White, C.J., Afargan-Gerstman, H., Muñoz, Á.G., Janiga, M.A., Vitart, F. et al. (2022. ISSN 0003-0007, 1520–0477) Advances in the subseasonal prediction of extreme events: relevant case studies across the globe. *Bulletin of the American Meteorological Society*, 103(6), E1473–E1501. Available from: https://doi.org/10.1175/BAMS-D-20-0221.1

Dorrington, J., Finney, I., Palmer, T. & Weisheimer, A. (2020. ISSN 0035–9009, 1477-870X) Beyond skill scores: exploring sub-seasonal forecast value through a case-study of French month-ahead energy prediction. *Quarterly Journal of the Royal Meteorological Society*, 146(733), 3623–3637. Available from: https://doi.org/10.1002/qj.3863

Fumo, N. & Rafe Biswas, M.A. (2015. ISSN 13640321) Regression analysis for prediction of residential energy consumption. *Renewable and Sustainable Energy Reviews*, 47, 332–343. Available from: https://doi.org/10.1016/j.rser.2015.03.035

Gelaro, R., McCarty, W., Suárez, M.J., Todling, R., Molod, A., Takacs, L. et al. (2017) The modern-era retrospective analysis for research and applications, version 2 (MERRA-2). *Journal of Climate*, 30(14), 5419–5454. Available from: https://doi.org/10.1175/JCLI-D-16-0758.1 Accessed on Mon, March 07, 2022.

Gonzalez, P.L.M., Brayshaw, D.J. & Ziel, F. (2021. ISSN 1477-870X) A new approach to extended-range multimodel forecasting: sequential learning algorithms. *Quarterly Journal of the Royal Meteorological Society*, 147(741), 4269–4282. Available from: https://doi.org/10.1002/qj.4177

Goutham, N., Plougonven, R., Omrani, H., Parey, S., Tankov, P., Tantet, A. et al. (2022. ISSN 1520-0493, 0027-0644) How skillful are the European subseasonal predictions of wind speed and surface temperature? *Monthly Weather Review*, 150(7), 1621–1637. Available from: https://doi.org/10.1175/MWR-D-21-0207.1

Guerrero, J.M., Vicuna, D., Garcia, L. & Uceda, J. (2007) Uninterruptible power supply systems provide protection. *IEEE Industrial Electronics Magazine*, 1(1), 28–38.

Guthrie, P. & Konaris, T. (2012) Infrastructure Resilience. page 24.

Kikstra, J.S., Mastrucci, A., Min, J., Riahi, K. & Rao, N.D. (2021. ISSN 1748-9326) Decent living gaps and energy needs around the world. *Environmental Research Letters*, 16(9), 095006. Available from: https://doi.org/10.1088/1748-9326/ac1c27

Li, J., Niu, D., Wu, M., Wang, Y., Li, F. & Dong, H. (2018. ISSN 1996-1073) Research on battery energy storage as backup power in the operation optimization of a regional integrated energy system. *Energies*, 11(11), 2990. Available from: https://doi.org/10.3390/en11112990

Li, M., Lu, J., Chen, Z. & Amine, K. (2018. ISSN 1521-4095) 30 years of lithium-ion batteries. *Advanced Materials*, 30(33), 1800561. Available from: https://doi.org/10.1002/adma.201800561

Millward-Hopkins, J., Steinberger, J.K., Rao, N.D. & Oswald, Y. (2020. ISSN 0959-3780) Providing decent living with minimum energy: a global scenario. *Global Environmental Change*, 65, 102168. Available from: https://doi.org/10.1016/j.gloenvcha.2020.102168

Mustafa, M.B., Keatley, P., Huang, Y., Agbonaye, O., Ademulegun, O.O. & Hewitt, N. (2021. ISSN 2352-152X) Evaluation of a battery energy storage system in hospitals for arbitrage and ancillary services. *Journal of Energy Storage*, 43, 103183. Available from: https://doi.org/10.1016/j.est.2021.103183

National Grid ESO. (2019) Response and reserve roadmap: report. Technical report.

National Grid ESO. (2020) GIS boundaries for GB DNO license areas. Technical report.

Peacock, M., Fragaki, A. & Matuszewski, B.J. (2023. ISSN 03062619) The impact of heat electrification on the seasonal and interannual electricity demand of Great Britain. *Applied Energy*, 337, 120885. Available from: https://doi.org/10.1016/j.apenergy.2023.120885

Schmidt, O., Melchior, S., Hawkes, A. & Staffell, I. (2019. ISSN 2542–4785, 2542–4351) Projecting the future Levelized cost of electricity storage technologies. *Joule*, 3(1), 81–100. Available from: https://doi.org/10.1016/j.joule.2018.12.008

Short, C.A., Guthrie, P., Soulti, E. & Macmillan, S. (2015) Health technical memorandum 07–02: EnCO2de 2015 – making energy work in healthcare. Technical Report 07-02, Department of Health, gov.uk.

Spry, W. (2023) Energy trends: UK renewables. https://www.gov.uk/government/statistics/energy-trends-section-6-renewables

Taylor, J.W. & Buizza, R. (2003) Using weather ensemble predictions in electricity demand forecasting. *International Journal of Forecasting*, 19(1), 57–70. Available from: https://doi.org/10.1016/s0169-2070(01)00123-6

Watson, H. (2022) How BT Group is making our networks more energy efficient. https://newsroom.bt.com/how-bt-group-is-making-our-networks-more-energy-efficient/

Weber, J., Wohland, J., Reyers, M., Moemken, J., Hoppe, C., Pinto, J.G. et al. (2018. ISSN 1932-6203) Impact of climate change on backup energy and storage needs in wind-dominated power systems in Europe. *PLoS One*, 13(8), e0201457. Available from: https://doi.org/10.1371/journal.pone.0201457

Weisang, G. & Awazu, Y. (2008) Vagaries of the euro: an introduction to ARIMA modeling. *Case Studies in Business, Industry and Government Statistics*, 2(1), 45–55.

White, C.J., Carlsen, H., Robertson, A.W., Klein, R.J.T., Lazo, J.K., Kumar, A. et al. (2017. ISSN 1350–4827) Potential applications of subseasonal-to-seasonal (S2S) predictions. *Meteorological Applications*, 24(3), 315–325. Available from: https://doi.org/10.1002/met.1654

SUPPORTING INFORMATION

Additional supporting information can be found online in the Supporting Information section at the end of this article.

How to cite this article: Fallon, J., Brayshaw, D., Methven, J., Jensen, K., & Krug, L. (2023). A new framework for using weather-sensitive surplus power reserves in critical infrastructure. *Meteorological Applications*, *30*(6), e2158. https://doi.org/10.1002/met.2158